Applied Catalysis A, General 621 (2021) 118174

Contents lists available at ScienceDirect

Applied Catalysis A, General

journal homepage: www.elsevier.com/locate/apcata

Strong impact of indium promoter on Ni/Al_2O_3 and Ni/CeO_2-Al_2O_3 catalysts used in dry reforming of methane

Anita Horváth [a,*], Miklós Németh [a], Andrea Beck [a], Boglárka Maróti [b], György Sáfrán [c], Giuseppe Pantaleo [d], Leonarda Francesca Liotta [d], Anna Maria Venezia [d], Valeria La Parola [d]

[a] Centre for Energy Research, Institute for Energy Security and Environmental Safety, Department of Surface Chemistry and Catalysis, Konkoly-Thege M. Street 29-33, H-1121, Budapest, Hungary
[b] Centre for Energy Research, Institute for Energy Security and Environmental Safety, Nuclear Analysis and Radiography Department, Konkoly-Thege M. Street 29-33, H-1121, Budapest, Hungary
[c] Centre for Energy Research, Institute of Technical Physics and Materials Science, Thin Film Physics Department, Konkoly-Thege M. Street 29-33, H-1121, Budapest, Hungary
[d] Institute for the Study of Nanostructured Materials, National Research Council (ISMN -CNR), Via Ugo La Malfa 153, 90146, Palermo, Italy

ARTICLE INFO

Keywords:
Methane dry reforming
Ni/Al_2O_3
Indium
Ceria
Coke formation

ABSTRACT

Herein, the promotion effect of only 0.3 wt% indium on 3% Ni/Al_2O_3 and 3% Ni/CeO_2-Al_2O_3 catalysts prepared by deposition-precipitation over a commercial alumina and on the CeO_2-modified support was studied. Catalyst characterization by XRD, TPR, XPS, TEM, CO-DRIFTS was performed. The catalytic properties were investigated and coke formation was analyzed under temperature ramped CH_4-decomposition and in Dry Reforming of Methane (DRM). The unique impact of indium was compared to the well-known effects of ceria additive. The carbon deposition on Ni/Al_2O_3 blocking the reactor could be only delayed due to ceria on Ni/CeO_2-Al_2O_3, while $NiIn/Al_2O_3$ was able to maintain the activity in DRM. Indium modifier acting in parallel with ceria over $NiIn/CeO_2$-Al_2O_3 determined the least coking, but the least catalytic activity. The results were discussed in terms of double role of In, acting as a ceria modifier, upgrading its oxidative properties and as a metal modifier, getting alloyed with Ni.

1. Introduction

The growing energy needs of mankind stimulate the utilization of unconventional methane resources such as shale gas, methane hydrates and renewable biogas. Furthermore, environmental regulations worldwide focus on the effective decrease of greenhouse gases in the atmosphere such as methane and CO_2. Combining these two important issues, methane conversion using CO_2 oxidant seems to be a sustainable way of getting value-added products from these abundant and relatively cheap starting materials. The so-called dry reforming reaction converts methane/biogas with CO_2 content and yields synthesis gas (DRM: $CO_2 + CH_4 \rightleftharpoons 2\ CO + 2\ H_2$). The synthesis gas is used for the production of value-added products such as methanol, acetic acid and hydrocarbons leading to end products such as solvents, polymers, synthetic fuels, fertilizers, etc. We should note that "dry" is used in contrast to the well-established industrial counterpart, the "steam" reforming of methane (SRM: $H_2O + CH_4 \rightleftharpoons CO + 3H_2$), which is the major hydrogen/syngas production route worldwide. Beside its extremely high investment and operational costs, if hydrocarbon synthesis is aimed, the $H_2/CO \sim 3$ ratio must be reduced. On the other hand, the CO-rich syngas of dry reforming represents a perfect source for the production of oxygenates or dimethyl ether [1]. The main disadvantage of catalytic DRM is that surface carbon easily accumulates in the form of filamentous or graphitic coke over the supported metal catalyst and this may lead to severe deactivation and the blockage of the reactor.

According to a very simple scenario of the DRM reaction steps, the methane dissociates on the metal surface to CH_x ($x = 0$–3) species, while CO_2 dissociates also on the metal or it is adsorbed and activated on the oxygen vacancies of the support at the metal-support interface, moreover, it can adsorb on remote support sites and decompose by hydrogen spillover from the metal. Then, active CH_x species react with O_s or OH_s species and decompose finally to H_2 and CO [2]. The surface CH_x species can polymerize and lead to inactive carbon, viz. filamentous or encapsulating type graphitic coke that eventually kill the catalyst. This

* Corresponding author.
E-mail address: horvath.anita@energia.mta.hu (A. Horváth).

https://doi.org/10.1016/j.apcata.2021.118174
Received 19 February 2021; Received in revised form 6 April 2021; Accepted 22 April 2021
Available online 29 April 2021

inactive carbon can potentially arise from methane decomposition and Boudouard reactions that compete for similar catalytic sites [3,4].

The cheapest and most perspective metal for methane dry reforming is nickel, however, it is prone to deactivation due to coke formation. The two general ways to reduce catalyst coking are i) the proper choice of support with mobile surface/subsurface oxygen (to boost carbon removal) and good CO_2 activation ability and ii) alloying nickel with a second metal [5]. As methane conversion is significant only above 500−600 °C, oxide supports with high specific surface area and good thermal stability are required, such as alumina, for example. As for the oxygen storage/release ability of the support, ceria component is an excellent and well-known choice: depending on the atmosphere (reducing or oxidizing), release or incorporation of oxygen species combined with Ce^{4+}/Ce^{3+} transformation can happen, and the mobile oxygen species can spill over to the neighboring metal sites where they gasify the carbon precursors [6]. The structure and extension of the metal-ceria interface and the proportion of Ce^{3+} sites play a crucial role in the activation of reactants and the gasification of active carbon species [7,8]. Oxygen transfer along the surface of CeO_2 support is fast but not selective for carbon oxidation only and so hydrogen species located at the proximity of the metal-support interface can be oxidized as well – forming water. This exhibits itself as a lower H_2 selectivity in dry reforming [9].

As for the metal modification, nickel must be modified, because it can form nickel carbide easily that is the starting point of nanotubes and graphitic layers. For economic reasons, non-noble metal modifiers are highly recommended. It was discovered in our laboratory that coke formation can be retarded by indium in close vicinity of nickel or rather by alloying with nickel [10]. The application of indium in catalysis is rather rare, and mostly the role of indium oxide in hydrogenation/dehydrogenation reactions is discussed [11–14]. Metallic indium in In/SiO_2 was found active in the direct dehydrogenative conversion of methane to ethane above 750 °C [15]. The combination of nickel with indium and alumina over SiO_2 provided a selective methanol producing catalyst via CO_2 hydrogenation [16]. During the electrochemical reduction of CO_2 [17] indium was found in partially oxidized state.

Our coke-resistant $3\%Ni2\%In/SiO_2$ catalyst contained less than 5 nm size bimetallic NiIn particles [10] giving a linear carbonyl band at 2013 cm^{-1} during CO chemisorption (DRIFTS) attributed to CO bonded on Ni atoms surrounded by In neighbors [18]. Methane pulse experiments on this catalyst revealed that the complete CH_4 dissociation was hindered [19].

Based on such dramatic effect of indium it seemed straightforward to test other supports such as alumina or alumina modified by ceria (that is often applied in reforming reactions for the above mentioned reasons [8, 20–23]) as the next generation of NiIn catalysts but with significantly lower indium content (~0.3 wt%). The ceria content of the mixed oxide was set reasonable low (~8 wt%) to induce as many as possible defect sites [21]. In the present work, the two different coke-reducing strategies were unified: i) we modified the thermostable support with defective, partially reducible cerium oxide in a low concentration and ii) doped the metal catalyst with minute amount of indium. We anticipated that the indium modifier will play a dual role as it can be alloyed with nickel and included in the supporting Al_2O_3 or CeO_2 matrix deliberately inducing oxide defects. These possibilities were analyzed in the present manuscript. Catalysts were investigated by TPR, BET, TEM, XPS and CO chemisorption DRIFTS experiments, while activity of the samples was tested in CH_4 decomposition and dry reforming reaction followed by coke quantification. The reasons for activity changes and coking properties were explained based on the results.

2. Experimental

2.1. Catalyst preparation

The ceria-modified alumina (CeO_2-Al_2O_3) support was prepared by wet impregnation of aqueous $Ce(NO_3)_3$*$6H_2O$ (Aldrich) solution on commercial alumina (Aldrich, SSA = 175 m^2 g^{-1}; V_p = 0.27 cm^3 g^{-1}) in order to have a final composition of 8.6 wt% CeO_2 (or 7 wt% Ce) on Al_2O_3. Once dry, the powder was calcined at 500 °C for 2 h in static air. The parent Al_2O_3 and the mixed CeO_2-Al_2O_3 support are referred as Al and CeAl from now on. Monometallic nickel and bimetallic nickel-indium catalysts were prepared by deposition-precipitation method on both supports (resulting Ni_Al, Ni_CeAl, NiIn_Al and NiIn_CeAl samples). The target metal loadings were 3 wt% Ni and 0.25 wt% In (nominal Ni/In molar ratio = 24). 1.5 g support and 2.5 g urea were suspended in 155 mL ultrapure water and stirred at room temperature until urea was dissolved. Then proper volume of 0.2 M nickel(II)nitrate (Aldrich) and – when needed – calculated amount of 0.06 M indium(III)chloride (Aldrich) were added. Then the temperature was ramped to 90 °C with 10 °C/min and the mixture was kept there for 3 h under stirring (final pH ~ 8.5). After cooling to room temperature, the sample underwent 3 cycles of centrifugation and washing steps. Catalyst samples were dried in an oven at 80 °C for 1 day, then calcined at 650 °C for 2 h in air flow (ex situ calcination). The calcined samples were further reduced ex situ at 750 °C/1 h in H_2 before DRIFTS, TEM and XPS measurements. This pretreatment is called ex situ reduction from now on.

2.2. Catalyst characterization methods

The bulk compositions of calcined Ni_CeAl and NiIn_CeAl samples were determined with non-destructive Prompt Gamma Activation Analysis (PGAA) technique at the neutron beam of the PGAA facility in Budapest [24,25]. The concentration calculation procedure is described by Révay [26].

The specific surface area and the pore volume of the samples were determined from N_2 adsorption–desorption isotherms at −196 °C using a Micromeritics ASAP 2020. Before measurements the samples were degassed at 250 °C for 2 h. The specific surface area was calculated through the Brunauer–Emmett–Teller (BET) method applied to the adsorption curve in the standard pressure range 0.05–0.3 P/P_0. By analysis of the desorption curve, using the BJH method, the mean pore size was obtained. The total pore volume (Vp) was evaluated on the basis of the amount of nitrogen adsorbed at the relative pressure of 0.95.

The crystalline structure of the calcined samples was determined by Powder X-ray diffraction patterns (XRD), performed on a Bruker D 5000 diffractometer equipped with a Cu K_α anode and graphite monochromator. The data were recorded in a 2θ range of 20°-80° with a step size of 0.05° and time per step of 5 s. The crystalline phases were analyzed by means of International Centre for Diffraction Data (ICDD) database.

Reduction properties of the calcined catalysts were studied by temperature programmed reduction (TPR) measurements in 5% H_2/Ar (30 mL/min) in the range between room temperature and 1000 °C with a heating rate of 10 °C/min. Experiments were carried out with a Micromeritics Autochem 2910 instrument equipped with a thermal conductivity detector (TCD). For each sample, about 0.1 g of powder was pre-treated in 5% O_2/He (30 mL/min) at 350 °C for 30 min and then cooled down under He atmosphere prior to the TPR run.

Morphology of the catalysts after ex situ calcination/reduction and after the DRM test reaction was investigated by Transmission Electron Microscopy (TEM) in TEM, HRTEM and HAADF modes by means of a FEI Titan Themis 200 kV spherical aberration (Cs) - corrected TEM with 0.09 nm HRTEM and 0.16 nm STEM resolution. Composition of the samples was measured by STEM-EDS and elemental maps were obtained by spectrum imaging with 4 Thermofischer "Super X G1″ EDS detectors built in the microscope.

In situ diffuse reflectance infrared Fourier transform spectroscopy (DRIFTS) was applied to study the adsorbed species detectable on the catalysts under 1% CO/Ar flow at room temperature. A Nicolet iS50 infrared spectrometer equipped with a Specac DRIFTS accessory and environmental chamber heatable up to 500 °C was used as detailed in [18]. After mounting the ex situ reduced sample on the sample holder, in situ reduction in the DRIFTS cell was carried out by heating the catalyst to 500 °C under 5% H_2/Ar atmosphere with 10 °C/min rate and kept at this temperature for 30 min then it was cooled down to room temperature ready for CO chemisorption. All spectra shown in here were corrected with the spectrum (background) taken just before the admission of CO.

Surface compositions of the samples were determined by X-Ray photoelectron spectroscopy (XPS) in a KRATOS XSAM 800 instrument. The samples were analyzed by using an unmonochromatized Al K-alpha source (1486.6 eV). The Al 2p binding energy from the alumina support set at 74.4 eV was used as reference for charge compensation. We believe that the alumina support can provide a good source for internal referencing, because both the shape and the FWHM of the Al 2p peak was the same in the samples and was not altered during the reduction pretreatments. The samples were measured after ex situ 650 °C calcination/750 °C reduction and after in-situ reduction at 500 °C for 30 min using 100 % H_2 inside the instrument's atmospheric pretreatment chamber. In some cases also the ex situ calcined (650 °C) state was measured. Because of the low amount of cerium and the overlapping of Ce $3d_{5/2}$ with the Ni $2p_{1/2}$ peaks, for evaluation of Ce^{3+} amount the data treatment of Pardo and his co-workers [27] was used. According to this method, the Ce(IV)% of cerium is estimated by calculating the attenuation of the u‴ component at 917 eV with respect to the total area of the Ce 3d peak after subtracting the Ni $2p_{1/2}$ contribution. The Ce^{3+} content in % was calculated according to Eq. (1).

$$\text{Ce(III)\%} = 100 - \text{Ce(IV)\%} = 100\text{-u}''' \text{ \%/14*100} \quad (1)$$

where u‴ is the area fraction of the peak at 917 eV. When there is only Ce^{4+} present in the sample (as in pure CeO_2), the u‴ peak is 14 % of the total area of the Ce 3d multiplet.

2.3. Catalytic studies

2.3.1. Methane activation experiments followed by thermogravimetric analyses of coke

The activation of methane by the catalysts was investigated through Temperature Programmed CH_4 decomposition (TP−CH_4) carried out using 50 mg of sample and a flow of 15 % CH_4/N_2 with 50 mL/min. The ex situ calcined catalysts before each TP−CH_4 experiment were oxidized first at 350 °C (30 min using 5% O_2/He and a ramp of 10 °C/min) than reduced at 750 °C for 1 h using 5% H_2/Ar and a ramp of 10 °C/min. The consumption of CH_4 was evaluated continuously in function of temperature by an IR analyzer (ABB Uras 26) calibrated in the range of 0–30 vol% for CH_4. The thermogravimetric analyses (TGA) of the samples after TP−CH_4 reactions were performed in air using the TGA 1 Star System of Mettler Toledo. About 10 mg of sample was heated from room temperature to 100 °C, left at this temperature for 1 h and then heated to 1000 °C at the rate of 10 °C/min in 30 mL/min of flowing air.

2.3.2. Catalytic DRM tests followed by temperature programmed oxidation of coke

The catalytic runs were done in a fixed-bed flow reactor at 1 atm using CH_4:CO_2:Ar = 49.5:49.5:1 mixture. 20 mg of catalyst along with 70 mg of diluting quartz beads were placed in a tubular quartz reactor where the reactant mixture was introduced at a flow rate of 70 mL/min (210 L/h/g_{cat}). At the beginning of the experiments, the ex situ calcined samples were in situ reduced first in 30 mL/min H_2:Ar = 90:10 mixture by heating from ambient temperature to 750 °C at a rate of 10 °C/min followed by a 1 h isothermal hold at the target temperature. Subsequently, the sample was cooled down to 650 °C in 10 min while it was purged with He, then the flowing gas was switched to the DRM mixture. Reaction was allowed to proceed for 6 h. A quadrupole Pfeiffer Prisma spectrometer was used for gas analysis and quantification of mass flow rates of H_2, CH_4, CO and CO_2 components were done in the way described in [10].

Temperature programmed oxidation (TPO) measurements after cooling the sample in He to room temperature were done in 40 mL/min O_2:He:Ar = 10:89:1 mixture under temperature ramp to 650 °C at a rate of 10 °C/min followed by a 30 min isothermal hold. CO_2 signal was used for quantification of carbon deposition removed after a calibration procedure.

3. Results and discussion

3.1. Structural characterization by N_2 adsorption, XRD, TPR and TEM

Bulk metal content of the calcined samples was measured by PGAA in two representative cases. Table 1 collects the theoretical and actual Ce, In and Ni content of the catalyst samples together with the particle size data to be discussed later on. As it is seen, Ce, In and Ni content corresponds well to the nominal values. The textural properties, viz. BET surface area, pore volume and pore size of the calcined samples were comparable, the CeO_2-modification induced only little decrease of surface area and pore volume compared to alumina, but metal introduction had no further effects (see Table S1).

Reducibility of the samples was investigated by Temperature Programmed Reduction (TPR) experiments in 5% H_2/Ar stream up to 1000 °C. The H_2-TPR profiles of the calcined catalysts are shown in Fig. 1. All the In and/or CeO_2 containing samples showed three main reduction peaks, at around 300 °C, 650 °C and 800 °C, labelled respectively as α, β, γ, while the monometallic Ni_Al represented reduction features only above 450 °C. The presence of reduction peaks at such a high temperature indicates strong interaction of NiO with the support [28,29]. The peak at ca. 650 °C (β) is attributed to highly dispersed NiO species interacting with the support via Ni-O-Al linkages [22] and the peak at temperature higher than 750 °C (γ) is attributed to $NiAl_2O_4$ [30,31]. Therefore, in the case of Ni_Al reference sample, a significant portion of nickel exists as strongly interacting NiO species over the alumina surface (reduction peak maximum at 660 °C) and similar amount of nickel is inserted into the alumina structure as surface or bulk probably non-stoichiometric $NiAl_2O_4$ (with peak maximum at 790 °C).

The presence of In promoter induced a small additional α peak at low temperature (270 °C) for NiIn_Al. According to literature reports, supported In_2O_3 usually shows two reduction zones, between 200−400 °C due to highly dispersed surface In_2O_3 species predominant at low indium concentration and between 500−800 °C due to reduction of bulk In_2O_3 [32–35]. In our catalyst this low temperature peak is assigned to the reduction of surface indium oxide species. The reduction of Ni-aluminate species shifts to slightly lower temperature (peak at 767 °C versus 790 °C of Ni_Al), this means Ni^{2+} in the alumina lattice is easier to reduce because of the close presence of indium (oxide). Thus, similarly to our previous findings [10], indium promoter somewhat modifies the interaction of NiO with the support, and here mixed Ni-Al-In-oxide compounds or islands were supposedly formed and reduced to Ni or NiIn particles.

The black curve in Fig. 1 represents the reduction of CeAl support. The presence of ceria additive with different reducibility is reflected by the small broad peaks in different temperature ranges. The low temperature peaks (at around 300 °C and 500 °C) are assigned to the reduction of surface CeO_2 species while the peak at 830 °C is characteristic of the bulk CeO_2 reduction [36]. If CeO_2 content on alumina is below 20–30 %, (that is the case here), and the reduction temperature is such high as here, we can suppose the formation of Ce_2O_3 reacting with Al_2O_3 and resulting finally a $CeAlO_3$ compound [36]. The Ni_CeAl

Table 1
Bulk composition and particle size data of the samples.

Sample name	Theoretical composition (wt%)			Elemental composition by PGAA (wt%)			Metal particle size by TEM (nm)	
	Ni	In	Ce	Ni	In	Ce	After red.	After DRM
Ni_Al	3	–	–	n.d.*	n.d.	n.d.	4.5 ± 1.3	n.d.
NiIn_Al	3	0.25	–	n.d.	n.d.	n.d.	5.1 ± 1.3	n.d.
Ni_CeAl	3	–	6.8	3.3	–	6.8	4.7 ± 0.9	5.8 ± 1.6
NiIn_CeAl	3	0.25	6.8	3.1	0.36	6.6	5.8 ± 1.6	6.6 ± 2.0

n.d.=not determined.

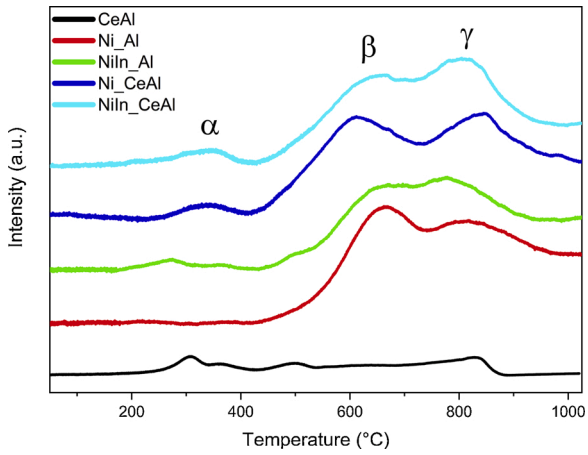

Fig. 1. TPR profiles of the calcined catalyst samples obtained under 5% H_2/Ar flow.

sample shows also a low temperature peak along with two high temperature peaks (β and γ). The α-feature can be assigned to the reduction of surface ceria interacting with surface Ni-oxide species. As found in other reports [37,38], the presence of ceria lowered the temperature of β peak (612 °C versus 660 °C) and consequently favored the reduction of surface NiO particles over Ni_CeAl. In contrast, the peak maxima of the Ni-aluminate species shifted 54 °C to higher temperature, meaning that a more-interacting [39] Ni-aluminate phase was formed when cerium oxide was also included in the support structure, yielding a sort of Ni-Ce-Al-oxide. Thus, it is harder to reduce nickel from this Ni-Ce-Al-oxide phase than from pure Ni-aluminate. The In-promotion in NiIn_CeAl sample brings the Ni-aluminate reduction peak to a lower temperature again (as in NiIn_Al compared to Ni_Al), while the presence of α peak shows the existence of some easily reducible Ni-CeO_x(-InO_y) compound on the alumina surface. Shortly, based on the above TPR results, the close vicinity of the modifier Ce-oxide or indium promoter to Ni is unambiguous.

Fig. S1 shows XRD pattern of calcined catalysts along with the respective Al (Al_2O_3) and CeAl (CeO_2-Al_2O_3) supports. In order to check the presence of NiO and/or $NiAl_2O_4$ found by TPR analysis, the reference patterns of those from ICDD database (00−044-1159 for NiO and 01−078-6950 for $NiAl_2O_4$) have been added to the graphics. Beside γ alumina, peaks of 7.4 nm sized crystalline cubic ceria could be also identified in CeAl. For all samples the diffraction patterns were analogous to the bare supports and no segregated crystalline NiO or $NiAl_2O_4$ were visible. We can postulate that after reduction treatment the metallic nickel particles were formed from this well-dispersed NiO species and (some of) the surface – probably non-stoichiometric – Ni-aluminate.

TEM and HRTEM images of the ex situ calcined and reduced samples gave information on the catalyst morphology, while colored EDS elemental mapping of chosen areas informed us on the distribution of Ni, Ce and In compounds. Our catalysts showed the presence of nickel particles with a very similar average particle size, between 4.5–5.8 nm (Table 1). The widest size distribution was observed on the most complex, NiIn_CeAl sample. Ni_Al catalyst is depicted in **Fig. S2**. A compact, kind of layered structure (**Fig. S2a**) and interplanar spacing of 0.46 nm corresponding to $NiAl_2O_4$ (111) phase was detected on the surface of Ni_Al sample along with some darker particles with 0.203 nm interplanar spacing assignable to Ni(111) (**Fig. S2b**). The surface coverage of alumina by the residual (not reduced) Ni-aluminate must be only partial, as the Ni content was low, and the majority of Ni-oxide must have been reduced during the reduction process at 750 °C. We suppose that relatively small Ni particles (~4.5 nm) on Ni-aluminate or alumina is the characteristic morphology of the Ni_Al sample prior to the DRM reaction (after calc650 °C/red750 °C treatment).

The indium-promoted counterpart of this sample (NiIn_Al, Fig. 2) has 5.1 nm size Ni particles and the same, compact, layered-like structure at some parts and thinner Ni-rich areas at other parts as well. (see the arrows in TEM image of Fig. 2**a** and the corresponding HAADF image in Fig. 2b). The HAADF image of such thinner area is shown in Fig. 2**c**. The colored EDS maps including Al, Ni and In in Fig. 2**d-f** prove that nickel is present in particulate form and indium is alloyed with nickel particles and dispersed also in/on the alumina matrix. Elemental mapping for this total area provides an average value of Ni/In~42 that is higher than the theoretical value (Ni/In = 24 or according to the elemental analysis Ni/In = 16), meaning that indium is not exclusively associated with nickel species. **Fig. S3** depicts the same thin area shown in Fig. 2c but with selected areas focused on several individual Ni particles, where the Ni/In atomic ratios were determined separately. All these and their average data were collected in a table beside the image. These data show that each of the Ni particles investigated is intimately associated with indium, viz. Ni is alloyed with indium. As the indium content is extremely low here, the detection of NiIn alloy based on lattice constant differences is really challenging and so to take HRTEM images were not in the focus of this work (Ni_2In and NiIn alloys in the 2%In3%Ni/SiO_2 sample were already found with ease [10]). Thorough investigation of the available TEM images with higher magnification resulted in the spot of lattice fringes shown in **Fig. S4**: the interplanar spacing of 0.212 nm might be attributed to the (102) or (110) plane of hexagonal Ni_2In alloy (PDF 42–1033).

The TEM image of Ni_CeAl sample is shown in **Fig. S5**. Similarly as above, a kind of ordered, compact areas can be observed along with groups of round particles, the darkest of them must be nickel. The ceria content did not cause significant difference in nickel particle size (4.7 ± 0.9 nm) but the size distribution slightly decreased, which indicates that the nickel-support interaction became stronger (remember the behavior of gamma peak in TPR spectra).

The presence of indium promoter over the mixed support increased the size of Ni particles and the size distribution widened. The TEM image of NiIn_CeAl in Fig. 3**a** shows both typical areas: thin, Ni-rich and a more compact structure with less nickel particles.

The thorough investigation of this sample revealed that ceria is not uniformly distributed over the catalyst (at least at nanoscale): there were ceria-richer (cloudy opaque area in the HAADF images) and ceria-leaner areas (Fig. 3**b-c**). In contrast, the distribution of indium is uniform and a value of Ni/In~25 was obtained all over the sample. It means that In is associated with nickel as it is shown by the colored elemental maps in as Fig. 3**d-e**. A closer, particle level distribution of Ni and In at higher

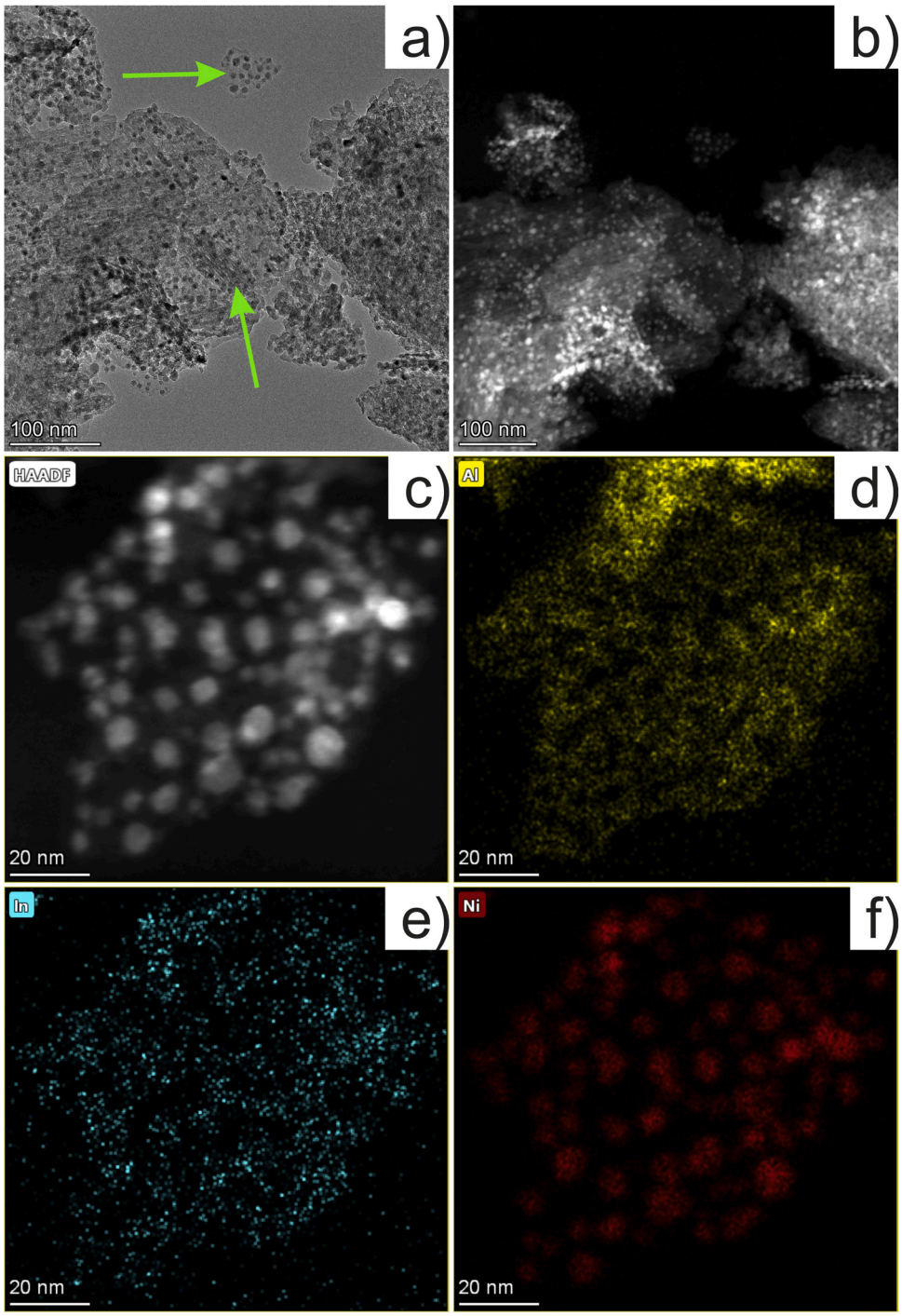

Fig. 2. TEM results of the calcined/reduced NiIn_Al sample: a) a thin Ni-rich area indicated by the upper arrow and a typical layered structure indicated by the lower arrow; b) HAADF image of the same area; c) HAADF image of a thin, Ni rich island and EDS elemental maps of d) Al, e) In and f) Ni elements obtained over this island.

magnification is shown again in Fig. S6. The composition of the individual particles was determined and collected in the table beside the figure and resulted exactly the theoretical Ni/In~24 composition as an average, meaning that In is present dominantly very close/inside/over each and every Ni particle. Comparing the Ni/In ratios of the two In-containing samples, we can suggest that indium is preferentially located in/around/on the nickel particles of the NiIn_CeAl sample (and more indium might be alloyed with metallic nickel than in NiIn_Al).

3.2. XPS characterization results

The XPS results collected in Table 2 provided valuable information on the oxidation state and surface concentration of catalyst components after the ex situ (750 °C) and then the in situ (500 °C) reduction treatment carried out inside the pretreatment chamber of the XPS machine. This “double reduction” was done to produce the same state of the catalyst that was formed in the high temperature reduction before the DRM reaction. Based on these considerations we exactly know the oxidation states and surface compositions present when contacting the reactants at the very beginning of the catalytic test.

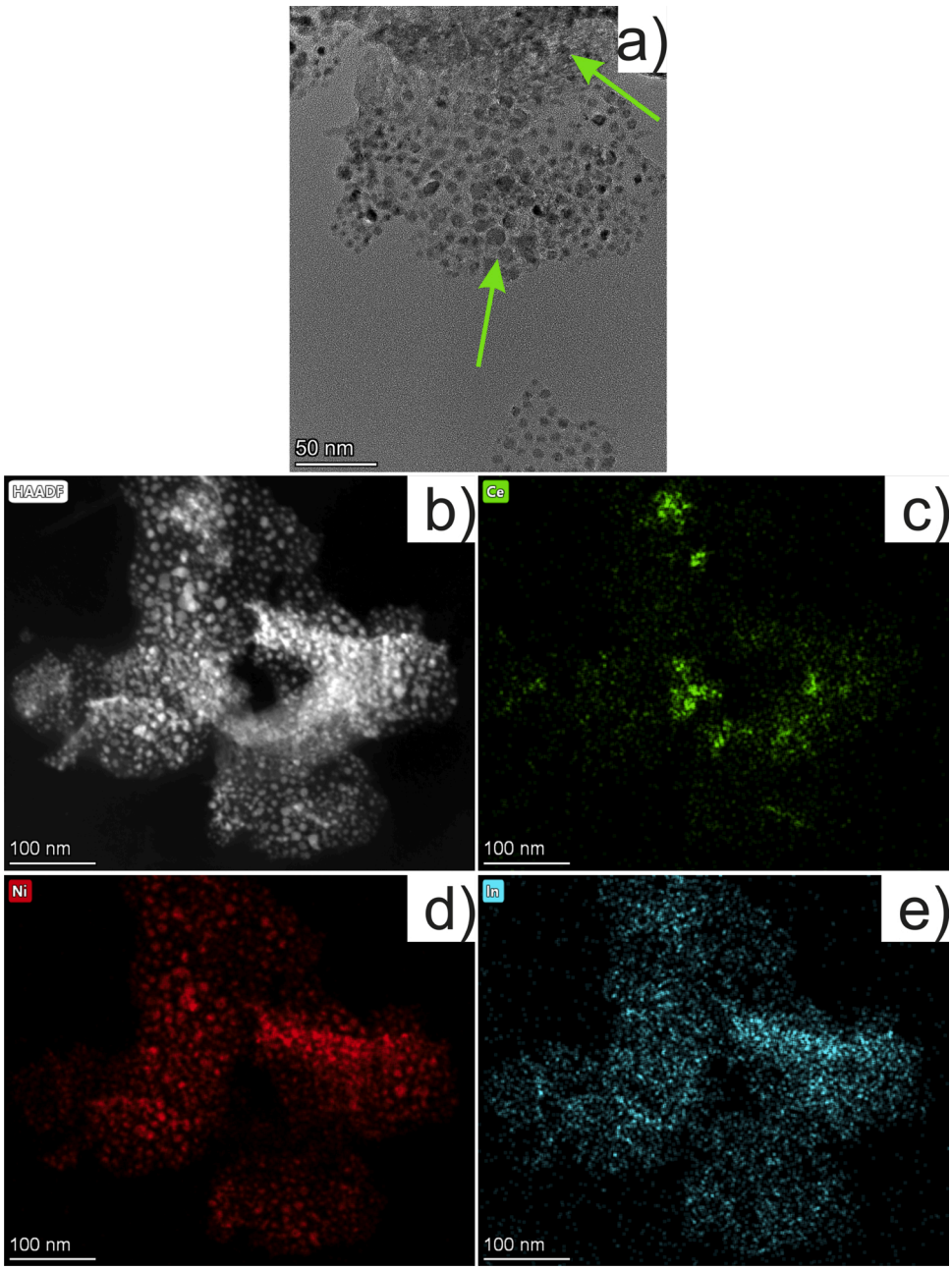

Fig. 3. TEM results of the calcined/reduced NiIn_CeAl sample: a) a typical layered structure indicated by the upper arrow and a thin Ni-rich area indicated by the lower arrow; b) HAADF image of a large area and EDS maps of c) Ce, d) Ni and e) In elements obtained over the same large area.

All catalysts showed very similar binding energy shifts and intensity changes that are detailed here using the spectra of two representative samples, NiIn_Al and NiIn_CeAl (Fig. 4**a-f**). As for the indium region, we have to keep in mind that there is maximum 1 eV difference in the BE of In° and In^{3+} The dotted line in Fig. 4**a-c** represents the shift of indium $3d_{5/2}$ peak position upon the reduction pretreatments. The peak with a maximum at 444.7 eV in calcined state of NiIn_Al (Fig. 4a) corresponds to indium oxide [40], which after the ex situ reduction shifted to 444.3 eV (not shown) and after the in situ reduction further to 444.0 eV (Fig. 4b) that is very close to the metallic indium detectable at 443.7 eV [41]. When Ce was present in the sample as in the case of NiIn_CeAl (Fig. 4c), the In peak in the in situ reduced state was located again at 444.1 eV. These low BE values suggest that after reduction significant amount (majority) of surface indium is present in zero oxidation state independent of the presence or absence of ceria additive.

Ni binding energy at 855.8 eV after ex situ calcination at 650 °C (Fig. 4d) corresponds to the presence of both Ni^{2+} in aluminate phase [42] and NiO_xH_y in the representative NiIn_Al sample [43]. The ex situ reduction produced a metallic nickel $2p_{3/2}$ component at 852.3 eV (not shown) that shifted with 0.2 eV downward upon the in situ reduction at 500 °C (852.1 eV), but a small fraction of Ni^{2+} remained, as the fitted green peak with 855.1 eV maximum reflects in Fig. 4**e**. We expected to find Ni^{2+} after the ex situ reduction treatment, because the sample surface was definitely re-oxidized by contact with ambient air after the H_2 treatment. The % Ni° column in Table 2 shows the ratio of metallic nickel among all nickel species, and it reflects nicely the sensitivity of nickel surface towards air (compare the ex and in situ reduced states for each catalyst). The extent of re-oxidation of Ni at room temperature is similar over both ceria containing samples and significantly higher than over the samples without ceria. Since TPR results implied that the ex situ reduction treatment at 750 °C is not able to reduce all the Ni-oxide to metallic state (being the last TPR peak maxima at higher temperature

Table 2
XPS results: surface composition data and relative amount of metallic nickel and Ce^{3+} sites.

#	Sample name	Atomic ratios				Ce^{3+}	Ni^0
		Ni/Al	Ce/Al	In/Al	Ni/In	(%)	(%)
1	Ni_CeAl_exsitu_red	0.56	0.031	–	–	15	25.8
2	Ni_CeAl_insitu_red	0.38	0.047	–	–	29	62.4
3	NiIn_CeAl_exsitu_red	0.26	0.049	0.019	13.3	37	26.5
4	NiIn_CeAl_insitu_red	0.19	0.064	0.016	11.8	51	66.0
5	NiIn_Al_exsitu_calc	0.28	–	0.037	7.42	–	0
6	NiIn_Al_exsitu_red	0.15	–	0.010	14.9	–	31.7
7	NiIn_Al_insitu_red	0.11	–	0.007	15.8	–	77.5
8	Ni_Al_exsitu_red	0.31	–	–	–	–	34.5
9	Ni_Al_insitu_red	0.25	–	–	–	–	62.7
10	CeAl_exsitu_calc	–	0.033	–	–	0	–
11	CeAl_exsitu_red	–	0.048	–	–	38	–
12	CeAl_insitu_red	–	0.053	–	–	60	–

than 750 °C), the presence of Ni^{2+} component (in the form of Ni-aluminate) – meaning the incomplete reduction of Ni-oxide – even after the lower temperature in situ reduction is highly acceptable. See that the highest reduced nickel amount was obtained over NiIn_Al that is 77.5 % (Table 2, entry 7). Note that in this sample the reduction of Ni-aluminate (γ peak in TPR) occurs at lower temperature than in the other catalysts.

If we follow the change of Ni and In surface concentrations during calcination and reduction of NiIn_Al sample (Table 2, entries 5–7), we can conclude that after calcination at 650 °C there are well dispersed nickel and indium oxide species on the surface that sinter upon reduction. The larger change in the corresponding In/Al versus Ni/Al values can be explained by enhanced indium sintering or diffusion into the bulk upon reduction. As the In BE values are close to that of the zero oxidation state, indium must be mostly metallic rather than included in the Al-O-Al matrix. Moreover, the TPR and STEM-EDS elemental mapping results also suggest that significant amount of In is associated (alloyed) with nickel.

Let us analyze now the XPS results concerning the state and distribution of Ce, since ceria component can play a significant role in the active oxygen transport and the coke removal during DRM reaction. The XPS cerium region in our case is more complex than usually because of the low amount of cerium and the overlapping with the Ni $2p_{1/2}$ peaks. The classic fitting suggested by Burrough [44] would have been complicated and uncertain here. This is why we used the method of Pardo [27] (see the Experimental and **Fig. S7**) for the determination of Ce^{3+} amount. The CeO_2-modified alumina support after calcination (Table 2, entry 10) contained fully oxidized ceria having only Ce^{4+} sites. The CeAl support after ex situ reduction at 750 °C and room temperature air contact shows a degree of reduction of 38 % (Table 2, entry 11). The subsequent mild in situ reduction, that influences mostly the upper

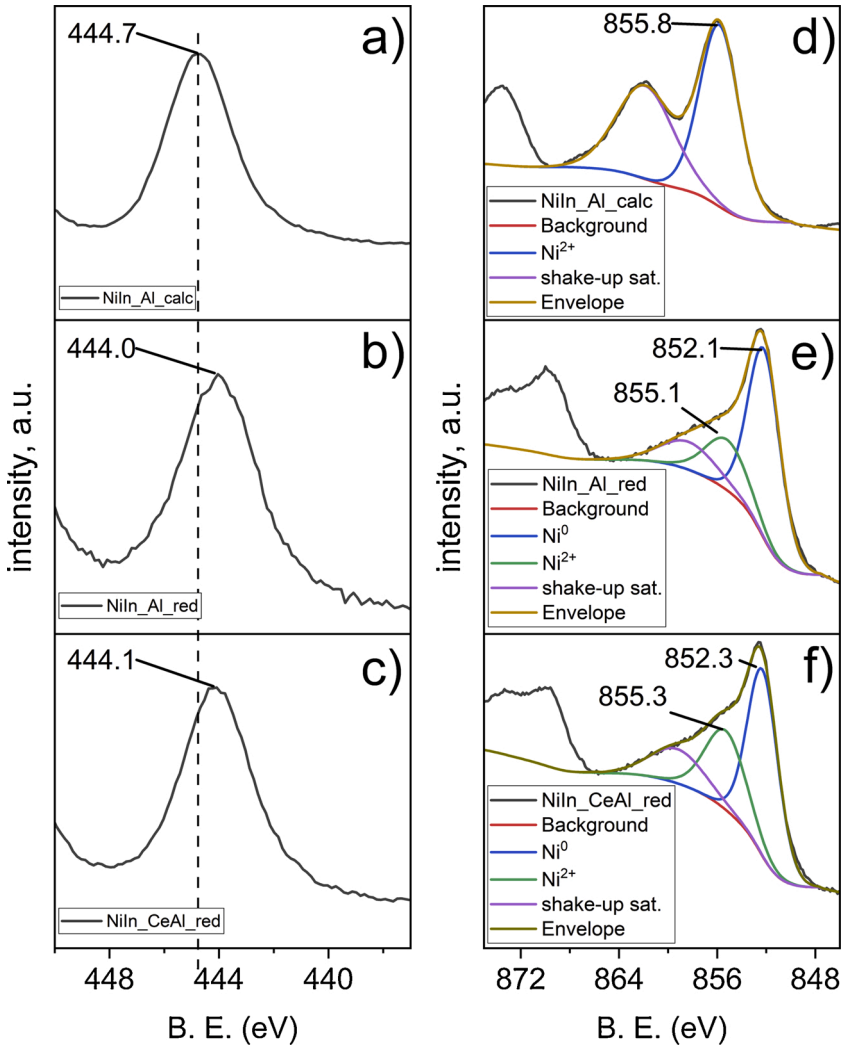

Fig. 4. Representative XPS results. Indium 3d region of a) NiIn_Al after ex situ calcination, b) NiIn_Al after in situ reduction and c) NiIn_CeAl after in situ reduction. Ni 2p region with the fitted Ni $2p_{3/2}$ components of d) NiIn_Al after ex situ calcination, e) NiIn_Al after in situ reduction and f) NiIn_CeAl after in situ reduction.

oxide/hydroxide layers but renders the sample into the same state as after the high temperature reduction, increases the reduction degree of surface ceria – and 60 % Ce^{3+} forms over the parent CeAl support (Table 2, entry 12). The addition of Ni or Ni with In by DP method caused a decrease of the final Ce^{3+} concentration compared to the parent CeAl support (compare entries 2, 4, 12 in Table 2). It is known that intrinsic oxygen vacancies are created upon the reduction of ceria with the concomitant formation of Ce^{3+} sites, and the increase of Ce^{3+} sites in the structure means the increase of the reducibility of ceria [6]. It seems that the reducibility of ceria modifier layer (its oxygen mobility) was decreased by the sole presence of nickel but only a little bit when indium guest ions were present as well. We should note that when a dopant (usually yttria) is incorporated in the ceria oxide lattice, additional oxygen can be removed from the material resulting the formation of extrinsic oxygen vacancies and a decrease of Ce^{3+} in the bulk structure [6]. This is why the amount of Ce^{3+} and the number of actual oxygen vacancies are not in strict relationship if guest atoms are expected to be incorporated in the ceria lattice. Unfortunately, our XPS oxygen spectra did not tell anything about the possible oxygen vacancies, as ceria content was really low and alumina oxygen was the prevailing component. However, no doubt, the highest Ce^{3+} concentration was obtained over the NiIn_CeAl catalyst sample.

The higher surface concentration of Ce (Ce/Al ratio) for the bimetallic NiIn_CeAl catalyst compared to Ni_CeAl suggests that different interactions and surface rearrangements took place over the same CeAl_support under the catalyst preparation and activation steps (DP and calcination/reduction). During the deposition-precipitation process the ideal case is that the precursor and the precipitant are distributed uniformly throughout the pores before the onset of slow precipitation by urea hydrolysis [45]. As the IEP of alumina is higher than that of CeO_2 [8] this may further vary the possibilities during deposition. To further complicate the picture, the calcination step transforms all components to different mixed Ni-(In)-Ce-Al-oxide species that reduce to metallic Ni (In) particles and some residual defective mixed surface oxide. Without knowing the exact reasons, it seems that ceria and nickel are distributed differently due to the indium promotion: there is more ceria on the surface and it is more reducible over NiIn_CeAl than over Ni_CeAl.

Finally, we should point out the surface In enrichment of NiIn_CeAl compared to NiIn_Al. If we accept that indium is present mainly in NiIn alloyed particles, the lower Ni/In ratio of NiIn_CeAl may suggest us that In is in higher concentration on the surface of its bimetallic particles.

The above XPS results tell us that Ni and In are mainly in metallic state after reduction, however, some oxidized Ni must be present and we cannot disclose minor amount of indium in oxidic state either. Note that the portion of nickel in zero oxidation state after the in situ reduction (~62 %) does not change when using the CeO_2-modified alumina instead of pure alumina. In contrast, indium promoter induces an increase in the metallic nickel ratio, the most for NiIn_Al (77.5 % Ni^0). This means ceria "rather keeps" nickel in oxidized state while indium enhances the amount of metallic nickel via its intimate contact or alloy formation with Ni, in accordance with the TPR results (remember the Ni-aluminate peak shifted to lower temperature for the NiIn samples).

3.3. CO chemisorption investigated by DRIFTS

The stretching frequency of CO in general depends on the nature of the adsorbing metal, its surface structure and the CO coverage [46]. DRIFT spectra were obtained on the reduced samples during CO chemisorption experiments using 1% CO/Ar mixture. The catalyst was "double reduced" to get as close as possible to the surface state present before the DRM test: the ex situ (750 °C) reduced samples were in situ pretreated at 500 °C in 5% H_2/Ar before the room temperature CO chemisorption in the DRIFTS cell.

Beside the gas phase CO absorption bands between 2100 and 2200 cm^{-1}, several bands of surface-bonded CO species can be seen in Fig. 5. The samples without indium exhibit less intense CO bands

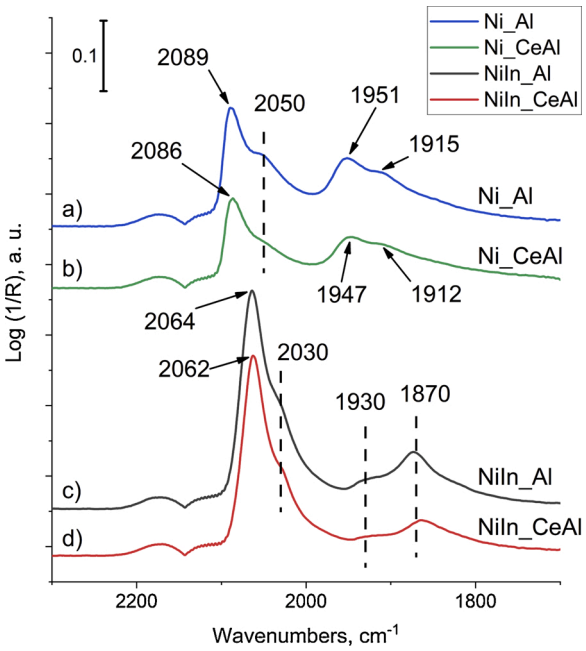

Fig. 5. DRIFT spectra of CO at room temperature over the in situ reduced samples in the presence of 1%CO/Ar. (Background corrected spectra are shown.).

(Fig. 5**a-b**). The band at around 2090 cm^{-1} (2089 cm^{-1} for Ni_Al and 2086 cm^{-1} for Ni_CeAl) is assignable to the CO molecules that are attached to the corner, step, kink Ni atoms of dispersed particles or to the presence of subcarbonyls [47,48]. The shoulder at around 2050 cm^{-1} can be assigned to chemisorbed monocarbonyls over dense facets [49, 50]. The band with a maximum at around 1950 cm^{-1} and a broad shoulder at around 1910 cm^{-1} can be attributed to bridge and multi-bonded carbonlys on low index planes with different surface heterogeneities (1951 cm^{-1} and 1915 cm^{-1} for Ni_Al and 1947 cm^{-1} and 1912 cm^{-1} for Ni_CeAl) [47,48]. The systematic 3–4 cm^{-1} red shift of each wavelengths in the case of ceria containing samples may reflect the small electronic effect of the Ni-ceria interface (increase of electron density of interfacial nickel via the formation of Ce^{3+} sites).

The same type of spectra for the indium-containing catalysts (Fig. 5**c-d**) present a strong red shift for all carbonyl bands and an enhanced ratio of linear/bridged CO species. Generally, if the electronegativity of a metal modifier is lower than that of nickel, it can cause an increase in the electron density of surrounding Ni sites and shift the CO peak to lower frequencies (red shift) [51]. While a small red shift of CO band of a bimetallic catalyst suggests that the modifier atoms disrupt the original metal ensembles and decrease the dipole-dipole coupling of adsorbed CO molecules (geometric effect) [52,53].

The ~30 cm^{-1} shift caused by the ~0.3 wt% In can be interpreted only if Ni is in close vicinity or rather alloyed with indium. The shortage of adjacent Ni sites due to the addition of In atoms would mean also the strong reduction, even the absence of bridged CO molecules (as was the case for our 3%Ni2%In/SiO_2 catalyst [18]). However, with as low as 0.3 wt% In here, calculating very roughly with Ni particles of 5 nm, the number of surface Ni atoms is still 4 times more than the indium atoms present in the sample and so even the theoretical monolayer coverage is not possible. It is indeed surprising how strong the indium effect is on the C≡O bond of chemisorbed carbonyls. The band that was seen at around 2090 cm^{-1} for the indium-free samples was shifted to ~2060 cm^{-1} (2064 cm^{-1} for NiIn_Al and 2062 cm^{-1} for NiIn_CeAl), and it is assigned to CO on Ni edge, corner, kink atoms surrounded by indium atoms. The small shoulder at around 2030 cm^{-1} must be attributed to CO bonded on bimetallic NiIn sites on closed packed planes, viz. Ni atoms surrounded by many or exclusively In neighbors. The band in the

bridged region at around 1870 cm^{-1} with a small shoulder at 1930 cm^{-1} for both In-containing samples is assigned to multiply bond carbonyls on Ni in contact with In-oxide at the metal-support interface.

Indium influences the bonding strength of CO drastically (see the large red shift). Additinally the dominance of the linear carbonyls at around 2060 cm^{-1} implies that indium deposition increases the ratio of undercoordinated Ni sites. That means the surface morphology of nickel particles must be very different: many Ni atoms are in defective, undercoordinated position – in the neighborhood of indium atoms.

3.4. Activity in CH_4 decomposition and the TGA results

The activity towards CH_4 activation was studied on reduced samples by Temperature Programmed CH_4 decomposition (TP−CH_4) up to 1000 °C. It is known that methane decomposition is a structure sensitive reaction and proceeds with higher activation energy over close packed than over open, undercoordinated planes of the metal [39]. Norskov et al. [54] demonstrated that step edges act as growth centers for graphene growth mainly because carbon binds more strongly to such sites than to sites on the close packed facets of Ni. It is clear that for CH_4 decomposition and DRM activity metallic nickel is required. We are aware of that our reduction pretreatment before these experiments was performed at 750 °C that is lower than the maximum of the γ TPR peaks. However, XPS results proved that significant part of the nickel content was reduced (up to 77 %) during 1 h reduction pretreatment at 750 °C and so there was metallic nickel present.

We expected different CH_4 decomposition profiles for our catalysts after detecting such big differences in the CO chemisorption wavelengths of In-promoted and unpromoted catalysts. The obtained TP−CH_4 curves are shown in Fig. 6.

All samples show basically the same feature: an initial small and a subsequent main dissociation peak. Nevertheless, there are differences in temperatures and in the amount of methane converted up to 800 °C as it is summarized in Table 3.

The starting points of methane dissociation ($CH_4 \rightleftharpoons CH_x + (4\text{-}x)H$), representing the light off values, followed the order: Ni_CeAl (390 °C) < NiIn_Al (430 °C), NiIn_CeAl (440 °C) < Ni_Al (520 °C). The lower light off temperatures found for the samples containing In and Ce may be related to the presence of different Ni(In)-InO_x-CeO_x interfaces. This assumption is supported by the relevant literature: experimental and theoretical results on Ni/CeO_2(111) surface showed that Ni atoms and small particles in direct contact with the ceria support are able to activate methane even at room temperature [55]. Although CH_4 dissociation proceeds generally on metallic Ni, interfacial O sites were also suggested as activation sites for methane dissociation [56]. In contrast,

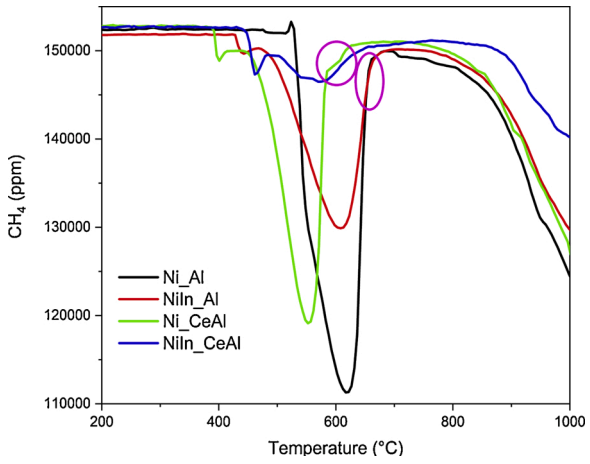

Fig. 6. Results of temperature programmed CH_4 decomposition experiments in the presence of 15 % CH_4/N_2 flow.

Table 3
Quantitative and qualitative results of temperature programmed CH_4 decomposition experiments.

Sample	Light off temp. (°C)	T of peak (°C)	Total CH_4 converted between 300−800 °C (mL)
Ni_Al	520	620	19.5
NiIn_Al	430	605	13.0
Ni_CeAl	390	550	15.5
NiIn_CeAl	440	570	5.5

$NiAl_2O_4$ phase was found to hinder or inhibit the adsorption and dissociation of CH_4 [57]. It is interesting to note for the Ce-free samples that the temperature of maximum CH_4 conversion was higher. The descending side of the four curves were paired into Ce-free and Ce-containing groups (circled in Fig. 6). This means the Ce-containing catalysts can activate methane at lower temperature but their activity ceased earlier supposedly due to deactivation by coking. The other two catalysts (Ni_Al and NiIn_Al) deactivated at higher temperature, and Ni_Al had the narrowest activity window. According to the literature, catalyst having the widest temperature window of CH_4 decomposition may exhibit the best anti-coking ability in dry reforming [58]. Based on this, Ni_Al is expected to be an easily coking catalyst. The most important issue of these experiments is that NiIn_CeAl sample converts the least CH_4 and seemingly has several activation sites with different nature.

The differences in the amount of converted methane calculated by the integration of the area between 300 and 800 °C may be related to differences in dispersion of the active phase that is roughly valid in our case as Ni_Al is the most dispersed while NiIn_CeAl the least one. However, beside the number of surface Ni atoms, their morphology and the presence of promoters have the same, or under our conditions, even more pronounced influence on the amount of decomposed methane. Theoretical calculations showed that substituting even subsurface Ni atoms of stepped surface with other elements can weaken the adsorption of atomic carbon, resulting in the change of reaction mechanism of methane decomposition [59]. Thus, if indium is located in the subsurface region of nickel, it can still influence CH_4 dissociation. The different profiles of the two In-containing samples emphasize the importance of ceria additive and/or suggest that different NiIn surfaces (Ni ensemble geometries) are present to dissociate the CH_4 molecules. (Although, this difference is not relevant at room temperature for the CO probe molecules.)

TGA analysis was performed after TP−CH_4 experiments in order to evaluate the amount and nature of carbon formed upon methane decomposition. Since the methane decomposition test was followed up to quite high temperature (1000 °C) and considering as well the effect of surface assisted gas phase reaction [58], the amount of deposited carbon must be handled with care. However, the TGA profiles, although miss quantitative information, they may still provide qualitative evidence of the coke nature. Fig. 7 depicts that oxidation of surface coke proceeds in two different temperature ranges (framed separately) reflecting the different typology and oxidation ability of carbon. Ni_Al shows a peak at ca. 675 °C and a shoulder at 625 °C typical for the oxidation of filamentous carbon having graphitic structure [60]. We assign the lower temperature shoulder to the oxidation of disordered, thin nanotubes and the main peak to thick, really tough nanotubes and crystalline coke, encapsulating the nickel particles. For NiIn_Al this last type of coke seems insignificant and mainly fine carbon nanotubes may have been formed. As for the Ce-containing samples, there was a first peak in the lower temperature range. In details, over NiIn_CeAl only a single peak was detected at ca. 410 °C, typical of amorphous carbon spatially closer to the active sites. This means that during CH_4 decomposition only a defective non-crystalline surface carbon was deposited that could be easily removed, in contrast with the other samples. Over the Ni_CeAl sample, two types of coke were deposited: an easily removable carbon at

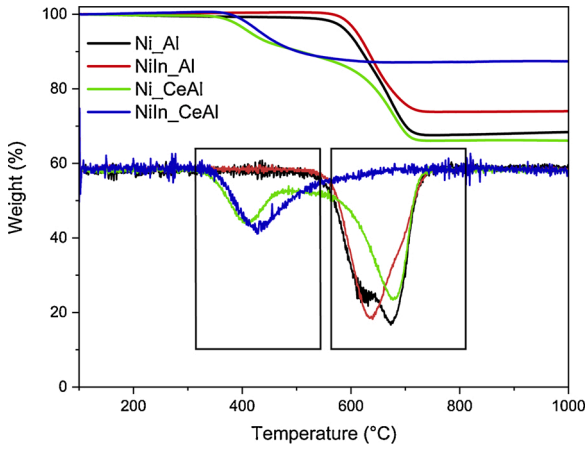

Fig. 7. TGA curves and their first derivatives after the TP−CH_4 experiments obtained during temperature ramp in the presence of airflow.

400 °C, and a tough, graphitic type with the typical peak at 680 °C. This implies that there might have been two types of active sites on Ni_CeAl: one of them may use the active oxygen provided by the ceria component [61,62], these are probably Ni atoms with Ni-CeO_2 interface (producing amorphous coke removable around 400 °C), while the other type is similar to the ones present on pure Ni_Al. The bulky, filamentous carbon is hard to remove as it usually moves under reaction and accumulates on the support surface far from the Ni active sites, or detaches the nickel particles terminating the metal support interaction.

These TGA experiments pointed out firstly that, in contrast with the pure alumina supported samples, the presence of cerium contributes to the creation of active sites promoting the deposition of easily removable carbon (as expected). The addition of indium to this system (NiIn_CeAl sample) inhibits substantially the CH_4 decomposition and produces only the easily oxidizable surface carbon. Adding indium to the pure alumina supported catalyst retards CH_4 decomposition in lower extent and has a pronounced effect on the morphology and/or the oxidation kinetics of graphitic coke.

3.5. Dry reforming of methane test reaction

3.5.1. Catalytic properties under dry reforming

The previous CH_4 decomposition experiments gave some hint on what trend in dry reforming activity could be expected. However, we know that the simultaneous presence of the reactants or the derived adsorbed species may influence the dissociation of the reactants themselves [63] and even the enhancement of carbon deposition can happen. Fig. 8 depicts the conversion curves obtained during DRM test reaction at 650 °C. All the samples exhibited decreasing reactant conversions under TOS.

The deactivation can be generally attributed to coke deposition, sintering or overoxidation of active Ni sites. The highest CH_4 conversion was obtained (42 %) over Ni_Al, while the lowest (25 %) over NiIn_CeAl catalyst. The Ni_Al and Ni_CeAl samples were so severely coked (see later) before the end of the test (TOS~6h = 360 min) that the mass flow controllers were not able to maintain the flow and the reaction must have been stopped before the end (this is why those conversion curves are shorter). Compared to the steeply descending curve of Ni_Al sample, the deactivation tendency was somewhat attenuated 10 min after the start of the reaction in the case of Ni_CeAl and the catalyst could convert methane up to 240 min. The slight decrease in the initial CH_4 and CO_2 conversions of this sample compared to that of Ni_Al could be explained with migration of reduced ceria from the support onto the Ni surface as in the case of a 5% Ni/CeO_2 [64]. (Remember, the lowest intensity CO band was found over this sample having the highest Ni concentration according to the XPS data.)

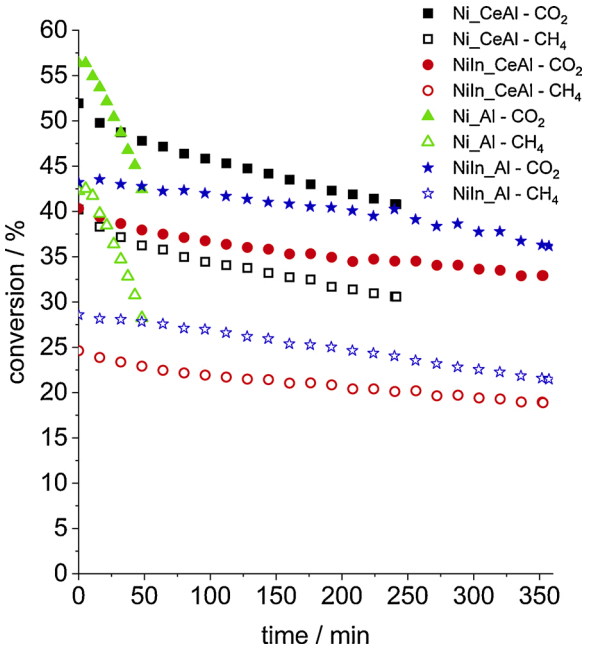

Fig. 8. Methane and CO_2 conversion curves during DRM test. CH_4: empty symbols, CO_2: full symbols. (Conditions: after reduction at 750 °C/1 h cooling to T = 650 °C in He, then DRM with CH_4:CO_2:Ar = 49.5:49.5:1 mixture, 210 L/h/$g_{cat.}$).

Concerning the In-promoted samples, the initial CO_2 and CH_4 conversion values were significantly lower, the least activity was presented by NiIn_CeAl, but they were much more stable than the In-free catalysts (CH_4 conversion over NiIn_CeAl decreased from 25 % to 19 % by the end of TOS). The lower initial CH_4 conversions reflect the decreased ability of NiIn surfaces to activate/dissociate CH_4, as the previous TP−CH_4 experiments showed (see Table 3), and are in agreement with the decrease of Ni dispersion values (TEM particle size, Table 1).

Table 4 collects the CO_2/CH_4 conversion and the H_2/CO ratios and the H_2 selectivity values obtained during DRM. The theoretical H_2/CO ratio is 0.8 under our conditions of 1 bar, stoichiometric reactants and 650 °C, the change of this ratio with TOS is shown in Fig. S8 for all our samples.

If H_2/CO is lower than the theoretical value, and the CO_2 conversion is higher than the CH_4 conversion, the occurrence of RWGS ($CO_2 + H_2 \rightleftharpoons CO + H_2O$) can certainly be assumed [65]. The data in the three columns of Table 4 should be correlated to understand the catalytic behavior of the samples. For the first thought, one would expect an increased CO_2 adsorption/activation/conversion due to the presence of basic CeO_2 component, but ceria modifier itself induced no increase in the initial CO_2/CH_4 conversion ratio compared to Ni_Al. As ceria has significant WGS activity even at moderate temperatures [66], this could influence the H_2/CO ratio obtained. The H_2 selectivity was the lowest for Ni_CeAl, which means the hydrogen atoms of methane were not fully converted to H_2 – some of them remained on the surface forming probably water or

Table 4
Catalytic results of DRM tests at 650 °C: conversion and H_2/CO ratios, H_2 selectivity.

Sample	CO_2/CH_4 conversion[a]	H_2/CO[b]	H_2 selectivity[c]
Ni_Al	1.33	0.68 → 0.64	0.90 → 0.93
Ni_CeAl	1.29	0.70 → 0.61	0.80 → 0.71
NiIn_Al	1.48	0.63 → 0.56	0.84 → 0.80
NiIn_CeAl	1.60	0.60 → 0.50	0.87 → 0.73

[a] At the beginning of the reaction.
[b] At the beginning and at the end of the reaction, see Fig. S8 for more details.
[c] At the beginning and at the end of the reaction.

surface OH groups.

When the indium promoter was present beside Ni, the CO_2/CH_4 conversion ratios increased. An excess CO_2 transformation occurred and H_2 selectivity was lower compared to Ni_Al, approving the formation of water and suggesting the occurence of RWGS as side reaction (H_2/CO ratio was lower than on Ni_Al). Note that In-oxide has itself some RWGS activity, which can be enhanced over In_2O_3-CeO_2 [67]. However, as indium loading is very low, and most indium is present in the bimetallic NiIn particles, we should attribute the RWGS activity to the surface Ni atoms of different nature: electronically perturbed and geometrically diluted by indium neighbors. CO bonding strength (DRIFTS results) and probably H_2 dissociation/adsorption strength (will be studied in the future) are altered compared to the pristine monometallic Ni sites. Moreover, InO_xH_y at the Ni-support interface can also play a role in this activity. The water forming during RWGS may efficiently contribute to the surface carbon gasification and coke removal.

3.5.2. *Coke deposition during dry reforming*

Table 5 collects the results of the subsequent TPO measurements giving information on the amount of deposited carbon and other characteristics of coke formation, such as the average carbon deposition rate and the C-selectivity (moles of deposited carbon /moles of converted $CO_2 + CH_4$ reactants till the end of the reaction). This latter is especially meaningful, because TOS varied among the catalysts. Although the most surface carbon was measured over Ni_CeAl (66 wt% C relative to the catalyst amount), this absolute value may be misleading due to the differences in the TOS. This is why the C selectivity in % can be used as a better measure for coking, and this value is definitely lower for Ni_CeAl than for Ni_Al.

This fact is certainly due to the presence of ceria modifier providing somewhat unselective oxygen pool for the gasification of surface carbon [55] and leaving the Ni sites active for reactant adsorption and conversion. Ceria modification of alumina in the present case was not sufficient to drastically reduce the coking tendency of nickel, while the sole or simultaneous presence of the indium promoter could eliminate the strong carbon buildup leading to reactor blockade.

Over the In-promoted samples the carbon deposition rate and carbon selectivity decreased by several magnitudes compared to the reference Ni_Al catalysts. The co-presence of ceria and indium additives produced the least coking but the least activity. This shows that there is a sensitive balance between activity and coking tendency and one has to focus on the development of a coking resistant catalyst with sufficient high activity. In this sense indium promotion alone seems to be more efficient than ceria addition.

The carbon content of the deposited carbonaceous materials shown in Table 5 was quantified by TPO experiments and typical TPO curves are seen in **Fig. S9** (Ni_CeAl and NiIn_CeAl). Although the amount was very different for the samples, the oxidation kinetics was very similar, all TPO curves had only one peak with a maximum at 650 °C, suggesting that mostly graphitic nanotubes were oxidized and contrary to the results after methane decomposition reaction, no amorphous carbon was formed. (Keep in mind that the CH_4 decomposition experiments started at much lower temperature when amorphous coke can be easily formed.) Thus, the amount of carbon determined in mg can be accepted as the weight of deposited coke, because mainly graphitic structures must have been formed based on the TPO analysis (and detected also by TEM, see later).

Table 5
Carbon deposition data, average carbon deposition rate and C-selectivity derived from TPO results after DRM.

Sample	TOS (min)	$C_{deposited}$/ $20mg_{cat}$ (mg)	$C_{deposited}$ (mmol/h)	C-selectivity, C_{dep}/ C_{conv} (%)
Ni_Al	48	8.61	0.897	1.08
Ni_CeAl	241	13.2	0.274	0.37
NiIn_Al	357	2.52	0.035	0.06
NiIn_CeAl	352	0.3	0.004	0.01

The TEM investigation of the spent, Ce-containing samples and that of the coke showed that the particle size of the spent samples increased only by 14–20 % (see Table 1) and the particle size distribution widened a bit for both samples. The relatively modest sintering can probably be attributed to the remaining Ni-aluminate moieties acting as a surface anchor for metallic nickel. Average Ni particle size below 10 nm is definitely favorable in order to decrease coking, thus thick graphitic layers around big crystalline nickel particles were not expected to be seen. The TEM images of Ni_CeAl sample shown in Fig. 9**a-b** represent several carbon nanotubes with different diameters ranging from 10 to 60 nm. Fig. 9**c** (rotated counterclockwise) shows the unified Al, Ni, Ce maps of the catalyst grain in Fig. 9**b**: we can see that Ni particles group close to each other at certain parts of the support. The aggregated Ni particles were not always overlapped with ceria "patches", viz. nickel-ceria interface was not apparently maximized. However, there were other catalyst grains (Fig. 9d) where nickel was well distributed over the support and the individual Ni particles (or NiO) kept distance.

TEM image of NiIn_CeAl in Fig. 10**a** depicts several thin nanotubes of maximum 18−20 nm width around a solid, layered-like catalyst grain and circumstanced by thin catalyst patches full of darker nickel(indium) particles. The two-type structure of the fresh catalyst could be found here as well. Fig. 10**b** and c shows the Al, Ce, Ni and In maps of the signed small territories in Fig. 10**a**.

The following statements can be drawn based on these images. Although nickel particles are larger with wider size distribution in the indium-promoted catalyst, they are better separated than over Ni_CeAl, but not always evenly dispersed over the support. Indium can be found mostly where Ni particles are located with an average Ni/In∼32 atomic ratio. The carbon nanotube (C map is not shown for clarity) with nickel at the tip in Fig. 10**c** contains low amount of indium (Ni/In∼66) that is apparently not enough to completely hinder carbide and nanotube formation but the particle at the tip is not covered so it remains active under DRM.

3.6. *The synergetic effect of indium and ceria as catalyst modifiers*

Based on the above results, we can rationalize the catalytic behavior by considering the interaction between the catalyst components. The final picture is valid only within the given concentration of CeO_2, Ni and In and for the synthesis method used. The big differences between the fast deactivating Ni_Al catalyst and the moderately active but almost coke-free NiIn_CeAl sample were not caused by the dissimilarity of Ni dispersion, because there is roughly only 20 % deviation in the average particle sizes. Moreover, unreduced Ni^{2+} is present in all the samples to quite a similar extent in the form of a surface Ni-aluminate, which can be responsible for the relatively small Ni particle size after a 750 °C reduction treatment. Catalyst surface area cannot play a role either, because BET surface area was above 100 m^2/g in all samples. The reducible ceria is a widely accepted catalyst component to decrease coking, but it was not sufficient itself in the present case: though the extensive coke formation was considerably reduced compared to that on Ni_Al sample, carbon plugged the reactor tube with time over Ni_CeAl as well. When promoting the Ni_Al catalyst with only ∼0.3 wt% indium, coke was remarkably decreased together with a drop in the initial CH_4 conversion from 42 to 28 %. The trend in terms of conversion decrease and enormously hampered coking was followed when ceria and indium additives were used simultaneously: NiIn_CeAl sample had a moderate activity forming only 1.5 % surface carbon during 6 h TOS. The slight deactivation on NiIn_CeAl sample can be explained by sintering and restructuring, as the average particle size increased a bit and the particle size distribution widened after the reaction (see Table 1). The deactivation is barely due to the carbonaceous coverage of the active sites, as the carbon selectivity was really low. Unfortunately we have no XPS results of the spent sample, and so the oxidation state of Ni and In after

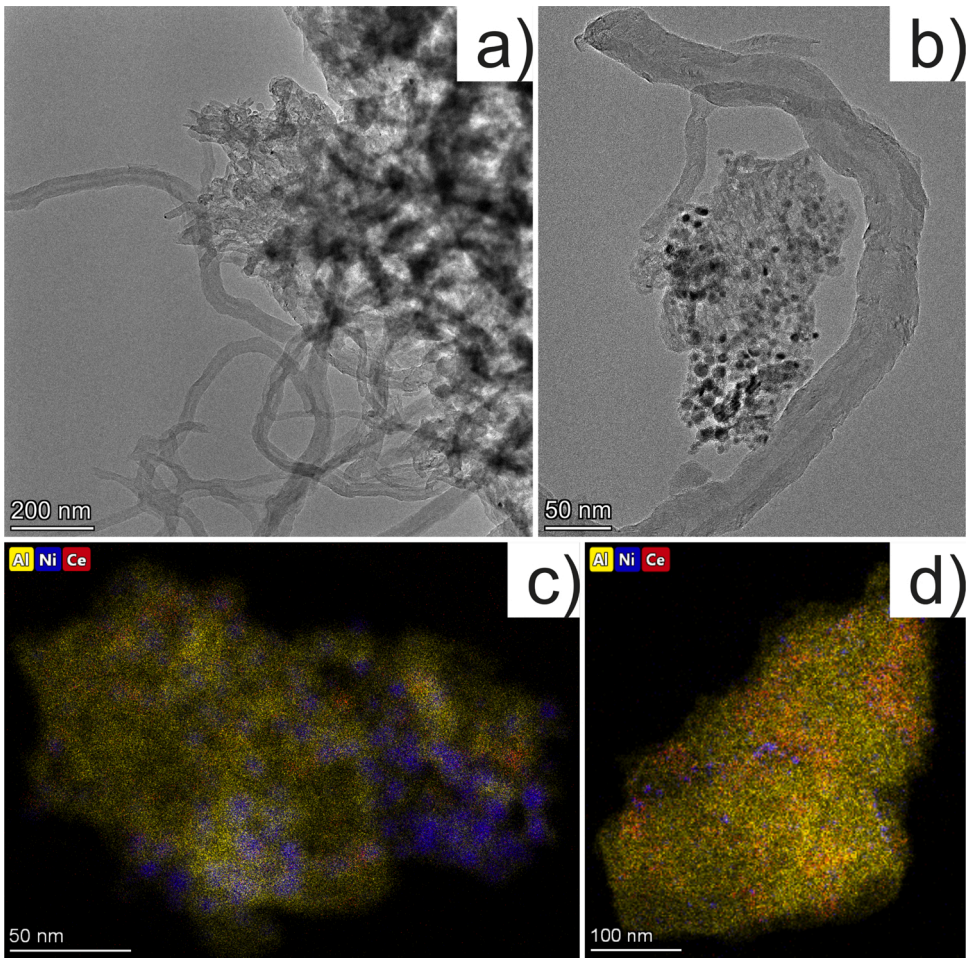

Fig. 9. TEM results of Ni_CeAl used in DRM test. a) Nanotube bundles of different diameter, b) a catalyst grain attached to a thick and a thin carbon nanotube, c) the colored EDS elemental maps of Al, Ni, Ce over the same catalyst grain as in b and d) another catalyst grain showing various Ni, Al, Ce distributions.

the reaction, the degree of nickel reoxidation (a possible reason for deactivation), if any, is not known.

The key to the understanding of catalytic behavior is the analysis of the possible interfaces and their dynamic interaction. In the systems with Ni, CeO_2, Al_2O_3 components, the metallic nickel is in contact with a mixed NiO-CeO_2-Al_2O_3 oxide. CH_4 dissociation starts easily but proceeds at a lower rate than over Ni_Al and due to the accessible oxygen pool provided by the ceria component, a lot carbon is gasified and leaves the nickel sites active, and so the fatal coke deposition is delayed. The key to this behavior is thought to be the presence of surface Ce^{3+} sites in the partially reduced CeO_2 or $CeAlO_3$-like species formed during prereduction or under reaction. This can activate CO_2 resulting CO and the oxidized CeO_2. This CeO_2 oxidizes then the CH_x species located at the Ni-support boundary and so the CeO_x/$CeAlO_3$ sites with Ce^{3+} are restored [68,69]. According to the literature, the formation of $CeAlO_3$ phase was found to significantly enhance carbon-resistance of the catalyst without decreasing the activity [69]. In our case the Ni/NiO-CeO_2-Al_2O_3 interface apparently was not large enough and carbon nanotube formation prevailed while some of the nickel was probably overoxidized (remember, Ni was easy to reoxidize in air, see XPS).

The indium promoter complicates the picture and induces new variables in the system: indium-oxide is able to finely spread over the alumina [35] and it can be incorporated in the CeO_2 lattice [70,71] as well, while the metallic indium can alloy with nickel. Lacombe et al. [72] investigated catalysts containing PtSn and 0.4 wt% In on Al_2O_3 prepared by two methods. Their XANES results showed that indium was mainly in the In^{3+} state in the support when coprecipitated, whereas it was mainly metallic In (alloyed with Pt or very close to it) when impregnated, but the blockade of Pt surface by indium was similar in both cases. Our results agree with this reference: in the reduced state of the catalyst, indium is alloyed with nickel, while a small amount is mixed with CeO_2 and alumina. It is accepted that Ce^{3+} sites exist mainly at the metal–ceria interface [6]. Indium incorporated in the ceria lattice increases the number of these Ce^{3+} sites and what is more they are more stable against oxidation in this interfacial ceria-indium-oxide providing additional new platform for CO_2 activation. The extra CO_2 transformation resulting in more reactive oxygen or H_2O via RWGS can further reduce catalyst coking on the expense of catalytic activity because the electronically perturbed surface nickel sites with indium neighbors are much less active in CH_4 dissociation, but on the other side, alloying Ni with indium can retard the harmful carbide formation. As during DRM reaction water is always present, it can oxidize metallic indium (in NiIn alloy) forming InO_xH_y or InO_x [73,74]. Indium-oxide can be reduced by H_2 [11,75] or CO [76] and on the partially reduced sites CO_2 dissociation can happen [12]. It is easy to see how many routes are available for CO_2 activation here.

Using alumina support modified with ceria, indium plays a double role firstly as a reducible oxide-modifier, secondly as a metal modifier. As a consequence, it decreases coking at a really low, 0.3 wt% indium content via a fine interplay between the In/InO_x over/around the nickel particles interacting with the CeO_x-Al_2O_3 matrix. We should point out once again that the lowered CH_4 conversion proves the existence of a new catalytic surface with less and electronically perturbed Ni atoms sterically isolated (or surrounded) by indium, because the metal particle

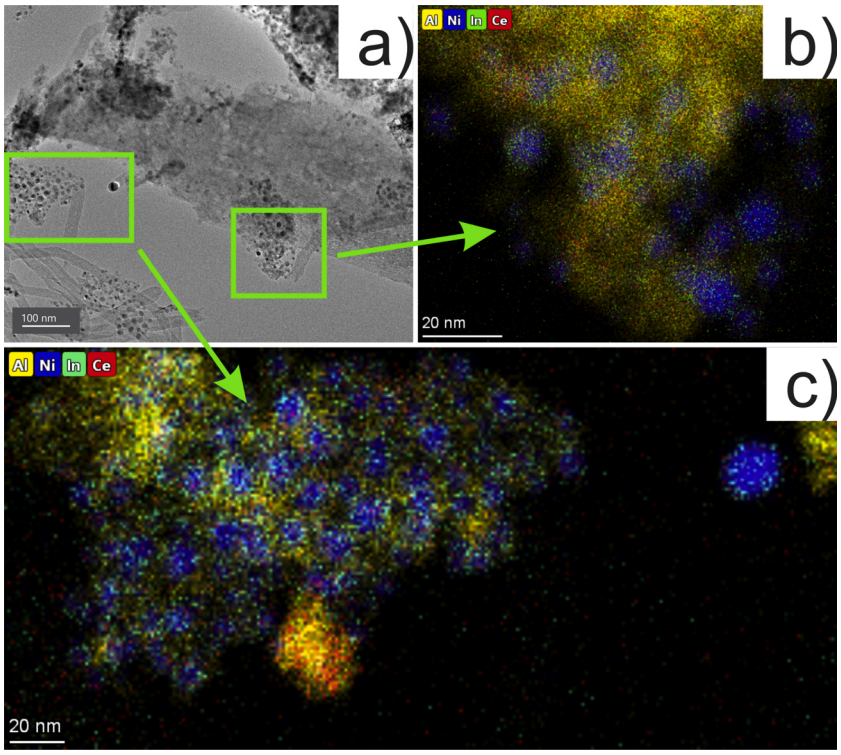

Fig. 10. TEM results of NiIn_CeAl used in DRM test. a) Thin carbon nanotubes and a catalyst grain with the typical layered territories and thin, Ni-rich areas marked with rectangles, selected for elemental mapping ; b) Al, Ni, In, Ce maps of the Ni-rich area enlarged from the rectangle on the right; and c) Al, Ni, In, Ce maps of the Ni-rich area enlarged from the rectangle on the left, with a metal particle of Ni/In~66 composition at the tip of a carbon nanotube (see the right top section of the image).

size was the same or very similar in all the four investigated samples. The DRIFTS results showed the presence of an electron-rich Ni in the bimetallic samples compared to monometallic Ni references and this seems to results in a decrease of DRM reactivity.

4. Conclusions

Herein, the parent 3% Ni/Al_2O_3 was modified with ceria or indium and both ceria and indium with a purpose to develop a new family of dry reforming catalysts. Indium was added by deposition precipitation together with nickel in a very low, 0.3 wt% concentration. The samples were investigated by several structural methods, while the catalyst activity was tested in a plug flow reactor at 650 °C in dry reforming of methane and during temperature ramped methane decomposition experiments, both coupled with coke quantification.

Independent of the composition, all samples had an average particle size between 4.5–5.7 nm in reduced state as determined by TEM. TPR and XPS suggested that indium promoted the reduction of nickel-oxide but some of the Ni^{2+} remained in the surface Ni-aluminate after reduction at 750 °C. Bimetallic NiIn particles were detected by STEM-EDS elemental mapping and CO-DRIFTS measurements, the latter suggesting the existence of electronic effects of indium. XPS proved that ceria had higher surface concentration with a higher number of Ce^{3+} centers after reduction due to indium promotion.

Temperature ramped CH_4 decomposition followed by TGA pointed out that NiIn_CeAl sample was the least active in CH_4 decomposition and produced only an easily oxidizable, probably amorphous surface carbon. In DRM test reactions at 650 °C, the co-presence of ceria and indium additives resulted the least coking and the least activity, but indium promotion alone caused still low coking at a higher activity. The more active Ni_CeAl coked heavily, and over the slightly more active Ni_Al catalyst the carbon deposition was even faster.

Based on all results, it is declared that over a 3%Ni0.3%In/CeO_2-Al_2O_3 catalyst, indium plays a double role as a reducible oxide-modifier, and also as a metal modifier and decreases coking at an extremely low In content via a fine interplay between the In/InO_x over/around the nickel particles interacting with the CeO_x-Al_2O_3 matrix.

CRediT authorship contribution statement

Anita Horváth: Conceptualization, Investigation, Writing - original draft, Writing - review & editing. **Miklós Németh:** Investigation, Methodology, Visualization, Writing - original draft. **Andrea Beck:** Methodology, Writing - review & editing. **Boglárka Maróti:** Investigation. **György Sáfrán:** Investigation. **Giuseppe Pantaleo:** Investigation, Visualization. **Leonarda Francesca Liotta:** Investigation, Visualization. **Anna Maria Venezia:** Supervision. **Valeria La Parola:** Conceptualization, Investigation, Writing - original draft.

Declaration of Competing Interest

The authors declare that they have no known competing financial interests or personal relationships that could have appeared to influence the work reported in this paper.

Acknowledgments

The financial support provided by the bilateral project between the Hungarian Academy of Sciences, Hungary and the National Research Council, Italy (HAS-CNR, Horváth/La Parola) is greatly acknowledged. The authors are grateful to Prof. A. Tungler (Centre for Energy Research) for his valuable comments. F. Giordano (ISMN-CNR) and N. Gallì (ISMN-CNR) for carrying out XRD and BET analyses are acknowledged.

Appendix A. Supplementary data

Supplementary material related to this article can be found, in the online version, at doi:https://doi.org/10.1016/j.apcata.2021.118174.

References

[1] J.R. Rostrup-Nielsen, J. Sehested, J.K. Nørskov, Advances in Catalysis, Academic Press, 2002, pp. 65–139, https://doi.org/10.1016/S0360-0564(02)47006-X.

[2] Y.-Z. Chen, B.-J. Liaw, W.-H. Lai, Appl. Catal. A Gen. 230 (2002) 73–83, https://doi.org/10.1016/S0926-860X(01)00996-6.
[3] M.A. Vasiliades, C.M. Damaskinos, K.K. Kyprianou, M. Kollia, A.M. Efstathiou, Catal. Today 355 (2020) 788–803, https://doi.org/10.1016/j.cattod.2019.04.022.
[4] M.A. Vasiliades, P. Djinović, L.F. Davlyatova, A. Pintar, A.M. Efstathiou, Catal. Today 299 (2018) 201–211, https://doi.org/10.1016/j.cattod.2017.03.057.
[5] D.G. Araiza, D.G. Arcos, A. Gómez-Cortés, G. Díaz, Catal. Today 360 (2021) 46–54, https://doi.org/10.1016/j.cattod.2019.06.018.
[6] J.B. Wang, Y.-L. Tai, W.-P. Dow, T.-J. Huang, Appl. Catal. A Gen. 218 (2001) 69–79, https://doi.org/10.1016/S0926-860X(01)00620-2.
[7] X. Yan, T. Hu, P. Liu, S. Li, B. Zhao, Q. Zhang, W. Jiao, S. Chen, P. Wang, J. Lu, L. Fan, X. Deng, Y.-X. Pan, Appl. Catal. B 246 (2019) 221–231, https://doi.org/10.1016/j.apcatb.2019.01.070.
[8] M.C. Alvarez-Galvan, R.M. Navarro, F. Rosa, Y. Briceño, F. Gordillo Alvarez, J.L. G. Fierro, Int. J. Hydrogen Energy 33 (2008) 652–663, https://doi.org/10.1016/j.ijhydene.2007.10.023.
[9] M.S. Aw, I.G. Osojnik Črnivec, P. Djinović, A. Pintar, Int. J. Hydrogen Energy 39 (2014) 12636–12647, https://doi.org/10.1016/j.ijhydene.2014.06.083.
[10] J. Károlyi, M. Németh, C. Evangelisti, G. Sáfrán, Z. Schay, A. Horváth, F. Somodi, J. Ind. Eng. Chem. 58 (2018) 189–201, https://doi.org/10.1016/j.jiec.2017.09.024.
[11] M.S. Frei, M. Capdevila-Cortada, R. García-Muelas, C. Mondelli, N. López, J. A. Stewart, D. Curulla Ferré, J. Pérez-Ramírez, J. Catal. 361 (2018) 313–321, https://doi.org/10.1016/j.jcat.2018.03.014.
[12] O. Martin, A.J. Martín, C. Mondelli, S. Mitchell, T.F. Segawa, R. Hauert, C. Drouilly, D. Curulla-Ferré, J. Pérez-Ramírez, Angew. Chem. Int. Ed. 55 (2016) 6261–6265, https://doi.org/10.1002/anie.201600943.
[13] X. Liu, W.-Z. Lang, L.-L. Long, C.-L. Hu, L.-F. Chu, Y.-J. Guo, Chem. Eng. J. 247 (2014) 183–192, https://doi.org/10.1016/j.cej.2014.02.084.
[14] M. Chen, J. Xu, Y.-M. Liu, Y. Cao, H.-Y. He, J.-H. Zhuang, Appl. Catal. A Gen. 377 (2010) 35–41, https://doi.org/10.1016/j.apcata.2010.01.011.
[15] Y. Nishikawa, H. Ogihara, I. Yamanaka, ChemistrySelect 2 (2017) 4572–4576, https://doi.org/10.1002/slct.201700734.
[16] A.R. Richard, M. Fan, ACS Catal. 7 (2017) 5679–5692, https://doi.org/10.1021/acscatal.7b00848.
[17] J.L. White, A.B. Bocarsly, J. Electrochem. Soc. 163 (2016) H410, https://doi.org/10.1149/2.0681606jes.
[18] M. Németh, F. Somodi, A. Horváth, J. Phys. Chem. C 123 (2019) 27509–27518, https://doi.org/10.1021/acs.jpcc.9b06839.
[19] M. Németh, G. Sáfrán, A. Horváth, F. Somodi, Catal. Commun. 118 (2019) 56–59, https://doi.org/10.1016/j.catcom.2018.10.003.
[20] P. Osorio-Vargas, N.A. Flores-González, R.M. Navarro, J.L.G. Fierro, C.H. Campos, P. Reyes, Catal. Today 259 (2016) 27–38, https://doi.org/10.1016/j.cattod.2015.04.037.
[21] S. Damyanova, J.M.C. Bueno, Appl. Catal. A Gen. 253 (2003) 135–150, https://doi.org/10.1016/S0926-860X(03)00500-3.
[22] P. Mierczynski, A. Mierczynska, R. Ciesielski, M. Mosinska, M. Nowosielska, A. Czylkowska, W. Maniukiewicz, M.I. Szynkowska, K. Vasilev, Catalysts 8 (2018) 380, https://doi.org/10.3390/catal8090380.
[23] N. Miletić, U. Izquierdo, I. Obregón, K. Bizkarra, I. Agirrezabal-Telleria, L.V. Bario, P.L. Arias, Catal. Sci. Technol. 5 (2015) 1704–1715, https://doi.org/10.1039/C4CY01438C.
[24] Z. Révay, T. Belgya, in: G.L. Molnár (Ed.), Handbook of Prompt Gamma Activation Analysis: With Neutron Beams, Springer US, Boston, MA, 2004, pp. 1–30, https://doi.org/10.1007/978-0-387-23359-8_1.
[25] L. Szentmiklósi, T. Belgya, Z. Révay, Z. Kis, J. Radioanal. Nucl. Chem. 286 (2010) 501–505, https://doi.org/10.1007/s10967-010-0765-4.
[26] Z. Révay, Anal. Chem. 81 (2009) 6851–6859, https://doi.org/10.1021/ac9011705.
[27] A. Pardo, S. Feliú, M.C. Merino, R. Arrabal, E. Matykina, Appl. Surf. Sci. 254 (2007) 586–595, https://doi.org/10.1016/j.apsusc.2007.06.036.
[28] Y. Gao, A. Aihemaiti, J. Jiang, Y. Meng, T. Ju, S. Han, X. Chen, J. Liu, J. Cleaner Prod 260 (2020), 120944, https://doi.org/10.1016/j.jclepro.2020.120944.
[29] R. Daroughegi, F. Meshkani, M. Rezaei, J. Energy Inst 93 (2020) 482–495, https://doi.org/10.1016/j.joei.2019.07.003.
[30] H. Wu, G. Pantaleo, V. La Parola, A.M. Venezia, X. Collard, C. Aprile, L.F. Liotta, Appl. Catal. B 156–157 (2014) 350–361, https://doi.org/10.1016/j.apcatb.2014.03.018.
[31] J. Lu, Y. Lei, G. Wan, Z. Mei, J. Yu, Y. Zhao, S. He, Y. Luo, Appl. Catal. B 263 (2020) 118177, https://doi.org/10.1016/j.apcatb.2019.118177.
[32] C.-Y. Chou, R.F. Lobo, Appl. Catal. A Gen. 583 (2019), 117144, https://doi.org/10.1016/j.apcata.2019.117144.
[33] P. Park, J. Catal. 210 (2002) 97–105, https://doi.org/10.1006/jcat.2002.3667.
[34] M. Fernández-García, E. Gómez Rebollo, A. Guerrero Ruiz, J.C. Conesa, J. Soria, J. Catal. 172 (1997) 146–159, https://doi.org/10.1006/jcat.1997.1842.
[35] M. Chen, J.-L. Wu, Y.-M. Liu, Y. Cao, L. Guo, H.-Y. He, K.-N. Fan, Appl. Catal. A Gen. 407 (2011) 20–28, https://doi.org/10.1016/j.apcata.2011.08.018.
[36] J.M. Rynkowski, T. Paryjczak, A. Lewicki, M.I. Szynkowska, T.P. Maniecki, W. K. Jóźwiak, React. Kinet. Catal. Lett. 71 (2000) 55–64, https://doi.org/10.1023/A:1010326031095.
[37] S. Damyanova, B. Pawelec, R. Palcheva, Y. Karakirova, M.C.C. Sanchez, G. Tyuliev, E. Gaigneaux, J.L.G. Fierro, Appl. Catal. B 225 (2018) 340–353, https://doi.org/10.1016/j.apcatb.2017.12.002.
[38] F. Mesrar, M. Kacimi, L.F. Liotta, F. Puleo, M. Ziyad, Int. J. Hydrogen Energy 43 (2018) 17142–17155, https://doi.org/10.1016/j.ijhydene.2018.07.104.
[39] X. Zhu, P. Huo, Y. Zhang, D. Cheng, C. Liu, Appl. Catal. B 81 (2008) 132–140, https://doi.org/10.1016/j.apcatb.2007.11.042.
[40] B.V. Crist, Handbook of Monochromatic XPS Spectra – Commercially Pure Binary Oxides, Vol. 2, XPS International LLC, California, USA, 2004, p. 184.
[41] B.V. Crist, Handbook of Monochromatic XPS Spectra – The Elements and Native Oxides, Vol. 1, John Wiley & Sons, Chichester, 2000, p. 133.
[42] Y. Choi, N.D. Kim, J. Baek, W. Kim, H.J. Lee, J. Yi, Int. J. Hydrogen Energy 36 (2011) 3844–3852, https://doi.org/10.1016/j.ijhydene.2010.12.081.
[43] M. Németh, D. Srankó, J. Károlyi, F. Somodi, Z. Schay, G. Sáfrán, I. Sajó, A. Horváth, Catal. Sci. Technol. 7 (2017) 5386–5401, https://doi.org/10.1039/C7CY01011G.
[44] P. Burroughs, A. Hamnett, A.F. Orchard, G. Thornton, J. Chem. Soc., Dalton Trans (1976) 1686–1698, https://doi.org/10.1039/DT9760001686.
[45] D.J. Draelants, Y. Zhang, H. Zhao, G.V. Baron, in: E. Gaigneaux, D.E. DeVos, P. Grange, P.A. Jacobs, J.A. Martens, P. Ruiz, G. Poncelet (Eds.), Scientific Bases for the Preparation of Heterogeneous Catalysts, Elsevier Science Bv, Amsterdam, 2002, pp. 159–165.
[46] G. Poncelet, M.A. Centeno, R. Molina, Appl. Catal. A Gen. 288 (2005) 232–242, https://doi.org/10.1016/j.apcata.2005.04.052.
[47] M. Agnelli, H.M. Swaan, C. Marquez-Alvarez, G.A. Martin, C. Mirodatos, J. Catal. 175 (1998) 117–128, https://doi.org/10.1006/jcat.1998.1978.
[48] M. Mihaylov, K. Hadjiivanov, H. Knözinger, Catal. Lett. 76 (2001) 59–63, https://doi.org/10.1023/A:1016786023456.
[49] R.G. Tobin, S. Chiang, P.A. Thiel, P.L. Richards, Surf. Sci. 140 (1984) 393–399, https://doi.org/10.1016/0039-6028(84)90740-4.
[50] A. Bandara, S. Dobashi, J. Kubota, K. Onda, A. Wada, K. Domen, C. Hirose, S. S. Kano, Surf. Sci. 387 (1997) 312–319, https://doi.org/10.1016/S0039-6028(97)00366-X.
[51] L.-C. de Ménorval, A. Chaqroune, B. Coq, F. Figueras, J. Chem. Soc., Faraday Trans. 93 (1997) 3715–3720, https://doi.org/10.1039/A702174G.
[52] K. Balakrishnan, A. Sachdev, J. Schwank, J. Catal. 121 (1990) 441–455, https://doi.org/10.1016/0021-9517(90)90252-F.
[53] Y. Yao, D.W. Goodman, Phys. Chem. Chem. Phys. 16 (2014) 3823–3829, https://doi.org/10.1039/C3CP54997F.
[54] S. Helveg, C. López-Cartes, J. Sehested, P.L. Hansen, B.S. Clausen, J.R. Rostrup-Nielsen, F. Abild-Pedersen, J.K. Nørskov, Nature 427 (2004) 426–429, https://doi.org/10.1038/nature02278.
[55] P.G. Lustemberg, P.J. Ramírez, Z. Liu, R.A. Gutiérrez, D.G. Grinter, J. Carrasco, S. D. Senanayake, J.A. Rodriguez, M.V. Ganduglia-Pirovano, ACS Catal. 6 (2016) 8184–8191, https://doi.org/10.1021/acscatal.6b02360.
[56] R.K. Singha, Y. Tsuji, M.H. Mahyuddin, K. Yoshizawa, J. Phys. Chem. C 123 (2019) 9788–9798, https://doi.org/10.1021/acs.jpcc.8b11973.
[57] A.E. Awadallah, M.S. Mostafa, A.A. Aboul-Enein, S.A. Hanafi, Fuel 129 (2014) 68–77, https://doi.org/10.1016/j.fuel.2014.03.047.
[58] M. Zhang, J. Zhang, Y. Wu, J. Pan, Q. Zhang, Y. Tan, Y. Han, Appl. Catal. B 244 (2019) 427–437, https://doi.org/10.1016/j.apcatb.2018.11.068.
[59] R.L. Arevalo, S.M. Aspera, M.C.S. Escaño, H. Nakanishi, H. Kasai, Sci. Rep. 7 (2017) 13963, https://doi.org/10.1038/s41598-017-14050-3.
[60] A.A. Abdulrasheed, A.A. Jalil, M.Y.S. Hamid, T.J. Siang, T.A.T. Abdullah, J. CO2 Util 37 (2020) 230–239, https://doi.org/10.1016/j.jcou.2019.12.018.
[61] V. La Parola, G. Pantaleo, F. Deganello, R. Bal, A.M. Venezia, Catal. Today 307 (2018) 189–196, https://doi.org/10.1016/j.cattod.2017.04.045.
[62] G. Pantaleo, V.L. Parola, F. Deganello, R.K. Singha, R. Bal, A.M. Venezia, Appl. Catal. B 189 (2016) 233–241, https://doi.org/10.1016/j.apcatb.2016.02.064.
[63] M.J. Hei, H.B. Chen, J. Yi, Y.J. Lin, Y.Z. Lin, G. Wei, D.W. Liao, Surf. Sci. 417 (1998) 82–96, https://doi.org/10.1016/S0039-6028(98)00663-3.
[64] C.M. Damaskinos, M.A. Vasiliades, V.N. Stathopoulos, A.M. Efstathiou, Catalysts 9 (2019) 621, https://doi.org/10.3390/catal9070621.
[65] M.K. Nikoo, N.A.S. Amin, Fuel Process. Technol. 92 (2011) 678–691, https://doi.org/10.1016/j.fuproc.2010.11.027.
[66] U. Oemar, Z. Bian, K. Hidajat, S. Kawi, Catal. Sci. Technol. 6 (2016) 6569–6580, https://doi.org/10.1039/C6CY00635C.
[67] W. Wang, Y. Zhang, Z. Wang, J. Yan, Q. Ge, C. Liu, Catal. Today 259 (2016) 402–408, https://doi.org/10.1016/j.cattod.2015.04.032.
[68] I. Luisetto, S. Tuti, C. Battocchio, S. Lo Mastro, A. Sodo, Appl. Catal. A Gen. 500 (2015) 12–22, https://doi.org/10.1016/j.apcata.2015.05.004.
[69] W. Chen, G. Zhao, Q. Xue, L. Chen, Y. Lu, Appl. Catal. B 136–137 (2013) 260–268, https://doi.org/10.1016/j.apcatb.2013.01.044.
[70] X. Chen, N. Deng, X. Zhang, J. Li, Y. Yang, B. Hong, D. Jin, X. Peng, X. Wang, H. Ge, H. Jin, J. Nanopart. Res. 21 (2019) 77, https://doi.org/10.1007/s11051-019-4516-3.
[71] M.Z. Naik, A.V. Salker, Mater. Chem. Phys. 212 (2018) 336–342, https://doi.org/10.1016/j.matchemphys.2018.03.043.
[72] A.N. Jahel, V. Moizan-Baslé, C. Chizallet, P. Raybaud, J. Olivier-Fourcade, J.-C. Jumas, P. Avenier, S. Lacombe, J. Phys. Chem. C 116 (2012) 10073–10083, https://doi.org/10.1021/jp301282r.
[73] Z.M. Detweiler, S.M. Wulfsberg, M.G. Frith, A.B. Bocarsly, S.L. Bernasek, Surf. Sci. 648 (2016) 188–195, https://doi.org/10.1016/j.susc.2015.10.026.
[74] K. Otsuka, A. Mito, S. Takenaka, I. Yamanaka, Int. J. Hydrogen Energy 26 (2001) 191–194, https://doi.org/10.1016/S0360-3199(00)00070-7.
[75] A.I. Serykh, J. Phys. Chem. C 120 (2016) 21436–21440, https://doi.org/10.1021/acs.jpcc.6b05681.
[76] K. Otsuka, T. Yasui, A. Morikawa, Bull. Chem. Soc. Jpn. 55 (1982) 1768–1771, https://doi.org/10.1246/bcsj.55.1768.